Available online at www.sciencedirect.com
ScienceDirect
C. R. Physique 7 (2006) 634–649
COMPTES RENDUS PHYSIQUE
http://france.elsevier.com/direct/COMREN/

Turbulent transport in fusion magnetised plasmas/Transport turbulent dans les plasmas magnétisés de fusion

Perturbative studies of turbulent transport in fusion plasmas

Paola Mantica [a,*], François Ryter [b]

[a] *Istituto di Fisica del Plasma, Euratom/ENEA-CNR Association, Via Cozzi 53, 20125 Milano, Italy*
[b] *Max-Planck-Institut für Plasmaphysik, EURATOM Association, Boltzmannstrasse 2, 85748 Garching bei München, Germany*

Available online 17 August 2006

Abstract

One powerful way to investigate transport is to study the dynamic plasma response to externally applied small perturbations. This article describes the experimental techniques and basic theory underlying the perturbative approach. It then reviews the most recent results on electron heat transport and discusses their interpretation based on key concepts from electrostatic turbulence theory. Finally it presents some hints for future extensions of the work. ***To cite this article: P. Mantica, F. Ryter, C. R. Physique 7 (2006).***

Résumé

Études perturbatives du transport turbulent dans des plasmas de fusion. Une puissante méthode d'investigation du transport dans les plasmas consiste à étudier sa réponse dynamique à une excitation extérieure. Cet article décrit les techniques expérimentales et la théorie de base de l'approche dynamique. Ensuite, les résultats essentiels obtenus sur le transport électronique de la chaleur sont décrits et leur interprétation est discutée sur la base des concepts déduits de la théorie du transport électrostatique turbulent. Finalement, de possibles futures extensions de cette méthode sont suggérées. ***Pour citer cet article : P. Mantica, F. Ryter, C. R. Physique 7 (2006).***

Keywords: Turbulent transport; Perturbative methods; Heat wave propagation; Electrostatic modes; Diffusivity; Convection

Mots-clés : Transport turbulent ; Méthodes perturbatives ; Propagation d'onde de chaleur ; Modes électrostatiques ; Diffusivité ; Convection

1. Introduction

It is common knowledge that more information concerning the physics of a phenomenon can be extracted from the analysis of its time dynamics than from a steady-state phase. This concept has been applied to the investigation of transport in plasmas for about 3 decades, with continuous refinement of experimental techniques and analysis methods and with many challenging results offered to theoretical work.

The rate of plasma energy rise following a step increase in an external power source was probably the first application of a transient in order to derive an estimate of the total coupled power, which is correct provided timescales much faster than those associated to transport mechanisms are considered. Analogously, and under the same assumptions,

* Corresponding author.
E-mail address: mantica@ifp.cnr.it (P. Mantica).

1631-0705/$ – see front matter
doi:10.1016/j.crhy.2006.06.004

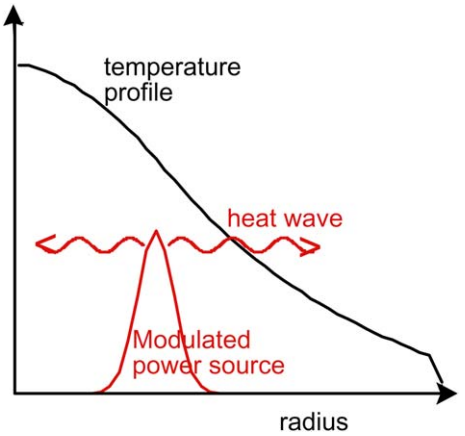

Fig. 1. Schematic drawing illustrating the basics of a heat wave propagation experiment using power modulation.

estimates of the profiles of deposited power density have been derived from the initial rate of increase of temperature at various radii (knowing the density profile), or equivalently from the analysis of the amplitude and phase of temperature fluctuations induced by a power modulation much faster than transport timescales. It has then been realized that considering slower time scales, even though detrimental for power deposition estimates, would bring precious experimental information on the transport mechanisms that determine the local response of temperature or density to a variation in the input source. From here, the step was short to consider the power source as a mere technique to provide what really matters in investigating transport, i.e., a heat or particle pulse (or train of pulses, so called 'heat wave') propagating through the plasma and diagnosing the plasma transport in a detailed way. This was obtained with a variety of sources, either externally applied at various locations (as in the schematic drawing in Fig. 1), or generated by the plasma itself through MHD instabilities expelling heat and particle pulses from the plasma core. Although the plasma response to a single pulse contains all physics information, wherever possible, periodic perturbations have been most commonly used, since they allow the reduction of noise levels by coherent averaging techniques.

Perturbative techniques have been applied to different transport channels. Electron heat transport has been the most extensively investigated as it is supported by powerful experimental tools. This will therefore be the main focus of the present article. For particle and impurity perturbative transport studies see, amongst others, [1–9]. Ion heat transport studies are extremely limited by the experimental possibilities.

For many years, the variety of results obtained from different machines using various types of perturbations, with findings in apparent contradiction with theoretical expectations and inconsistencies between machines or techniques, has represented a serious challenge to the understanding of transport. In recent years, a consistent interpretation of the results has emerged, based on the key concept provided by the theory of plasma electrostatic instabilities: the existence of a threshold above which transport increases, with an intensity that depends on various plasma parameters, including the temperature itself and its gradient, as described in the introductory chapter of this Issue [10]. This concept, besides providing a unified explanation for many previously inexplicable experimental results, has triggered more focused experiments that have further demonstrated the validity of the approach. Therefore, the bulk of perturbative transport results can be reasonably explained by the physics basis of electrostatic turbulence. Some exceptions exist that may call for more sophisticated models, as discussed in the following.

The purpose of this article is to describe the state of art of perturbative studies of turbulent heat transport, focusing on the electron channel. Since the publication of previous reviews on this topic [11–14], much more insight into the physics interpretation of perturbative experimental findings has been gained. In Section 2, the basics of perturbative methods are reviewed, together with a description of key theoretical concepts that have recently guided perturbative transport work. In Section 3 an overview of results for electron heat transport in conventional scenarios is provided, whilst Section 4 deals with some initial results in plasmas characterized by the presence of Internal Transport Barriers. Section 5 discusses open issues and possible future extensions of perturbative methods. Section 6 contains some conclusions.

2. The basics of perturbative transport methods

2.1. Transport equations

The basic system of coupled equations that govern heat and particle transport in a plasma can be written as

$$\begin{aligned} &\frac{\partial n_e}{\partial t} + \nabla \cdot \Gamma_e = S_e \\ &\frac{\partial (\frac{3}{2} n_{e,i} T_{e,i})}{\partial t} + \nabla \cdot (\mathbf{q}_{e,i} + \tfrac{5}{2} T_{e,i} \Gamma_{e,i}) = Q_{e,i} \end{aligned} \tag{1}$$

where $n_{e,i}$ is the plasma (electron or ion) density, $T_{e,i}$ is the (electron or ion) temperature, $\Gamma_{e,i}$ and $\mathbf{q}_{e,i}$ the (electron or ion) particle and heat fluxes, S_e and $Q_{e,i}$ the particle and (electron or ion) heat sources and sinks. n_i, the main ion density, is linked to n_e and to the impurity densities via the quasi-neutrality condition.

The relation between fluxes and thermodynamic variables or their gradients can be generally written as

$$\mathbf{F} = -\mathbf{D}\nabla\mathbf{u} + \mathbf{V}\mathbf{u} \tag{2}$$

where

$$\mathbf{F} = \begin{pmatrix} \Gamma_e \\ \mathbf{q}_e/n_e \\ \mathbf{q}_i/n_i \end{pmatrix}, \qquad \mathbf{u} = \begin{pmatrix} n_e \\ T_e \\ T_i \end{pmatrix} \tag{3}$$

and $\mathbf{D}$ and $\mathbf{V}$ are the matrices of the transport coefficients corresponding to diffusive and convective components of the fluxes:

$$\mathbf{D} = \begin{bmatrix} D_e & c_{12} & c_{13} \\ c_{21} & \chi_e & c_{23} \\ c_{31} & c_{32} & \chi_i \end{bmatrix}, \qquad \mathbf{V} = \begin{bmatrix} v & a_{12} & a_{13} \\ a_{21} & U_e & a_{23} \\ a_{31} & a_{32} & U_i \end{bmatrix} \tag{4}$$

Here D_e is the electron particle diffusivity, v the electron particle convection, $\chi_{e,i}$ the (electron or ion) heat diffusivity, $U_{e,i}$ the (electron or ion) heat convection (negative sign means inward pinch) and the c's and a's coefficients express the coupling between the various thermodynamic variables. We note that it has often become practice to call 'convective' also terms coming from off-diagonal transport, because in the transport equation (Eq. (1)) they appear in front of the first spatial derivative of the transported quantity rather than in front of the second spatial derivative, but it is more rigorous to make a distinction between off-diagonal and convective transport.

For a small perturbation of the thermodynamic variables, $\tilde{\mathbf{u}}$, Eqs. (1) and (2) can be linearized, leading to linearized transport equations for perturbations of the form

$$\frac{\partial \tilde{\mathbf{u}}}{\partial t} = \mathbf{A}\nabla^2\tilde{\mathbf{u}} - \mathbf{B}\nabla\tilde{\mathbf{u}} - \mathbf{C}\tilde{\mathbf{u}} + \mathbf{S} \tag{5}$$

where $\mathbf{A}$, $\mathbf{B}$, $\mathbf{C}$ are respectively the matrices of perturbed diffusivities, convection velocities and damping terms and $\mathbf{S}$ are sources/sinks. These are the coefficients that govern the time/space evolution of a perturbation. In general, the coefficients in $\mathbf{A}$ and $\mathbf{B}$ differ from the ones contained in $\mathbf{D}$ and $\mathbf{V}$ in Eq. (4), if the coefficients in $\mathbf{D}$ and $\mathbf{V}$ depend on the thermodynamic variables and their gradients, as discussed in [15].

To illustrate this, we consider the simple case of a purely diffusive electron heat flux in which χ_e depends on ∇T_e. Then the equation for $\tilde{T}_e$ would be governed by a perturbed χ_e, χ_e^{pert}, given by the incremental heat diffusivity

$$\chi_e^{\text{pert}} = -\frac{\partial q_e}{n_e \partial \nabla T_e} = \chi_e + \frac{\partial \chi_e}{\partial \nabla T_e} \nabla T_e \tag{6}$$

which is generally different from the power balance electron heat diffusivity χ_e^{pb}

$$\chi_e^{\text{pb}} = -\frac{q_e}{n_e \nabla T_e} \tag{7}$$

if the relation between fluxes and gradients is non-linear, as first pointed out in [16] and illustrated in Fig. 2.

These considerations indicate that the combined analysis of χ^{pb} and χ^{pert} yields the most complete information on transport.

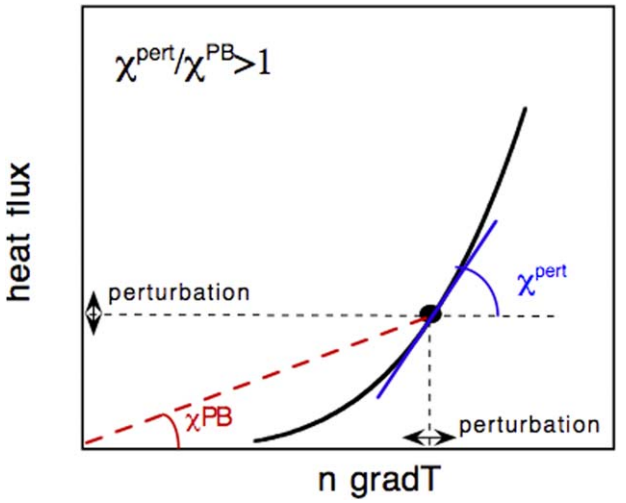

Fig. 2. Schematic representation of the difference between perturbative and power balance χ in the case that the heat flux is a non-linear function of the temperature gradient (after [12]).

2.2. *Basic formulae for perturbed transport coefficients*

As described in [17], considering harmonic temperature perturbations of the form $\tilde{T} = T_\omega e^{i\omega t}$, with $T_\omega = Ae^{-i\varphi}$ (A and φ being the amplitude and phase of the temperature perturbation), then in infinite slab geometry the slopes of the A and φ profiles in a source-free region for a purely diffusive plasma are related to χ^{pert} by a simple relation:

$$\chi^{\text{pert}} = \frac{3/4\omega}{-\varphi' A'/A} \tag{8a}$$

This relation expresses the fact that in plasmas with high χ^{pert} heat waves propagate quickly and with little attenuation, whilst with low values of χ^{pert} heat waves are strongly damped and slowed down. Cylindrical geometry introduces corrections on the amplitude term, yielding a commonly used relation, valid sufficiently far from the axis and the edge of the plasma:

$$\chi^{\text{pert}} = \frac{3/4\omega}{-\varphi'(A'/A + 1/2r - 1/2r_n)} \tag{8b}$$

where r is the radial coordinate and $r_n = -n_e/\nabla n_e$. The slopes of A and φ separately yield two values

$$\chi^A = \frac{3/4\omega}{(A'/A + 1/2r - 1/2r_n)^2} \quad \text{and} \quad \chi^\varphi = \frac{3/4\omega}{\varphi'^2} \tag{9}$$

which can be used to quantify the behaviour of A and φ profiles and spot anomalies from simple diffusive behaviour, for which $\chi^A \leqslant \chi^\varphi$, the difference being due to additional damping terms (e.g., due to collisional electron–ion coupling or Ohmic source modulation following resistivity modulation) that vanish at high frequency [17]. We note that Eqs. (8a) and (8b) yield a valid estimate of χ^{pert} also in the presence of a finite damping term, whose effect cancels out in the product of phase and amplitude derivatives. So these relations assume only zero convection and source free region. More general formulae for the case with convection have been derived in [17] and their application relies on availability of multi-frequency data, since the effect of convection decreases with increasing frequency.

Depending on the localization of the source, two types of approaches are used to analyse perturbative experiments. In the case of a localized perturbation source, when it is possible to determine the slopes of A and φ in a source-free region, Eq. (8b) yields the value of χ^{pert}. The comparison with χ^{pb} provides information on the properties of the transport mechanisms at work. Ideally, this analysis should be performed at various frequencies, allowing us also to determine the perturbed convection velocity as described in [17]. An alternative approach, applicable to cases with localized or non-localized modulated power, is to perform a full transport simulation of the experiment, assuming a space- and time-dependent model for the heat diffusivity and convection. In this case either the source profile is

well known or multi-frequency measurements are needed in order to work out the power deposition profile as well as transport. When empirical models with adjustable coefficients are used, best fit of time-averaged profiles and amplitude and phase profiles allows to reach quantitative estimates of transport as well as to test key physics ideas on transport mechanisms at work. When 1st principle based transport models (see chapter 3 of this issue [18]) are used, comparison of simulation results and data allows us to judge the validity of a model in a more stringent way than using pure steady-state results.

2.3. Basics on turbulent transport

As described in previous chapters of this issue [10,18], electron heat transport can be driven by TEM, ITG and/or ETG micro-instabilities, which become unstable above respective thresholds, which include, in particular, the normalized temperature gradient.

This can be represented in a very simple transport model initially successfully applied to ASDEX Upgrade data [19] and extended later as described in [20]:

$$\chi_e = \chi_s q^{3/2} \frac{T_e}{eB}\frac{\rho_s}{R}\left[R\frac{|\nabla T_e|}{T_e} - \left(R\frac{|\nabla T_e|}{T_e}\right)_{\text{crit}}\right]^{\alpha} \cdot H\left[R\frac{|\nabla T_e|}{T_e} - \left(R\frac{|\nabla T_e|}{T_e}\right)_{\text{crit}}\right] + \chi_0 \frac{T_e}{eB}\frac{\rho_s}{R} \tag{10}$$

This model is graphically illustrated in Fig. 3(a), and (b). The heat diffusivity χ_e increases from a basic level, not necessarily neoclassical, to a higher level induced by turbulent transport, when a critical value $(R/|\nabla T_e|/T_e)_{\text{crit}}$ is exceeded. H is the Heaviside step-function which provides the threshold effect above $(R/|\nabla T_e|/T_e)_{\text{crit}}$. The residual transport term is quantified by the dimensionless parameter χ_0, whilst χ_s quantifies the turbulent term, which, being proportional to the slope of the heat flux curve above threshold, yields the level of stiffness of temperature profiles. For large χ_s values, an increase of the heat flux drives a large increase in χ_e and therefore does not result in a change of $(R/|\nabla T_e|/T_e)$, thereby leading to stiff temperature profiles. The normalization factor $(T_e\rho_s)/(eBR)$ in both terms reflects the gyro-Bohm character of transport and introduces a temperature dependence $T_e^{3/2}$ in χ_e. The dependence on q, the safety factor, is introduced to recover the experimentally observed dependence of confinement on plasma current. The coefficients χ_s, α, χ_0 and the threshold are adjusted to fit the data best. An analytical expression for χ_e^{pert} can be easily derived from this formula [32]. The behaviour of χ_e and χ_e^{pert} is sketched in Fig. 3(b). χ_e^{pert} features a discontinuity at the threshold, which can be identified by heat wave propagation. In the following we will refer to this model as the 'CGM' (Critical Gradient Model).

Under conditions with dominant electron heating with $T_e > T_i$, at low collisionality, electron transport is most likely driven by TEM driven turbulence (see for instance [21]). The ITG modes contribute very weakly and the ETG modes are stable: this situation provides ideal conditions to study electron heat transport and TEM modes properties. The above empirical model is therefore well suited to take into account the basic physics phenomena. It does not

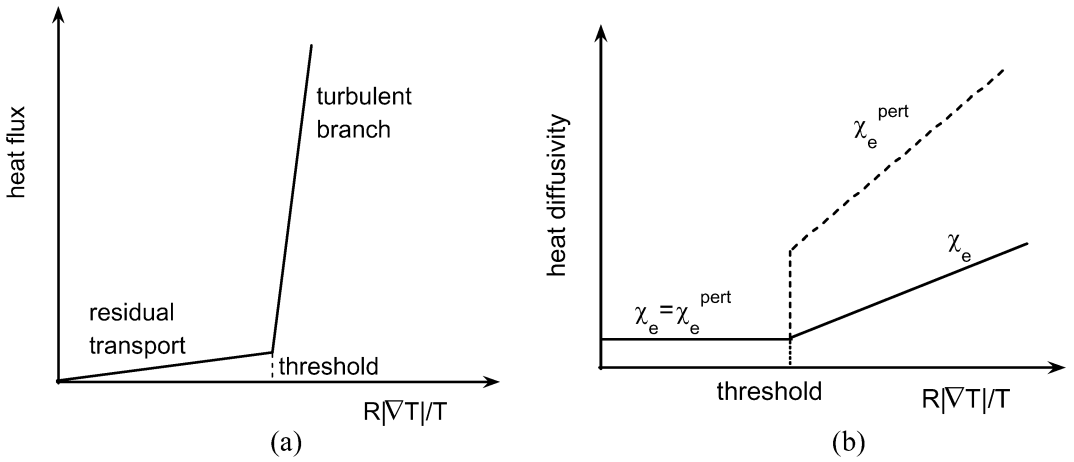

Fig. 3. Schematic diagram of (a) the dependence of the heat flux on the inverse temperature gradient length and (b) the behaviour of heat diffusivity with inverse temperature gradient length, in a critical gradient based model.

pretend to take into account the complete transport physics but it is a useful tool to investigate the validity of the hypothesis and to compare different plasmas and machines.

2.4. Experimental perturbative techniques and limitations

The first technique employed for heat pulse propagation studies made use of the heat and particle pulses expelled from the plasma core following an MHD crash, typically that associated with sawtooth activity [22]. More recently, cold pulses generated at the edge by ELMs and propagating to the centre have also been used [23]. One drawback of MHD generated heat pulses is, however, that MHD crashes perturb the magnetic configuration, enhancing the heat transport diffusivity via mechanisms that have nothing to do with the background heat transport. This leads to a ballistic type of heat propagation in a region whose extension is not clearly determinable, leading to overestimated values of χ^{pert} over a large fraction of the radius [24]. Therefore, this technique is now rarely used.

Heating power modulation is probably the most widely used technique. Power is usually square wave modulated with various choices of duty-cycle and modulation depth, to provide a spectrum with several harmonics of the modulation frequency. Standard FFT analysis of the T_e time traces is then applied to extract profiles of amplitude and phase of the heat wave. Amplitudes are small compared to the temperature. The use of many cycles, and cross-correlation with power, yield good signal to noise ratio. By far the best option for electrons is to use Electron Cyclotron Resonance Heating (ECRH), especially with 2nd harmonic X-mode, which guarantees 100% direct and localized heat deposition to electrons (see, e.g., [25]). The location of power deposition is also easily controlled either by steering beams poloidally or by adjusting the toroidal field value. Fig. 4 shows typical time traces for an ECH modulation experiment on ASDEX Upgrade with off-axis ECH deposition, and Fig. 5 shows the associated A and φ profiles at several harmonics.

Alternatively, Ion Cyclotron Resonance Heating (ICRH) power has been used in JET where ECH is not available. In minority heating scheme this has however the drawback of a rather broad profile, of delivering power simultaneously to electron and ion channels, and in an indirect way through fast ions, whose slowing down time is typically 50–200 ms.

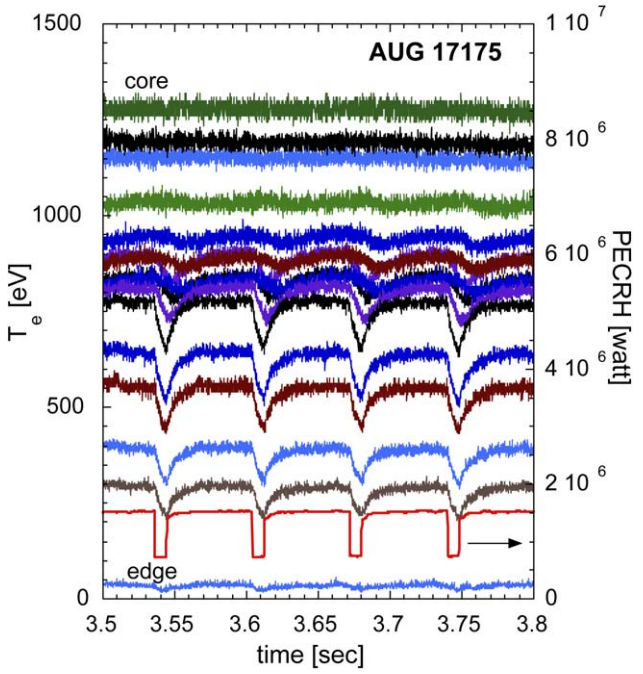

Fig. 4. Experimental T_e and ECH power (in red) time traces for a modulated discharge with ECH deposition at $\rho = 0.6$ in ASDEX Upgrade.

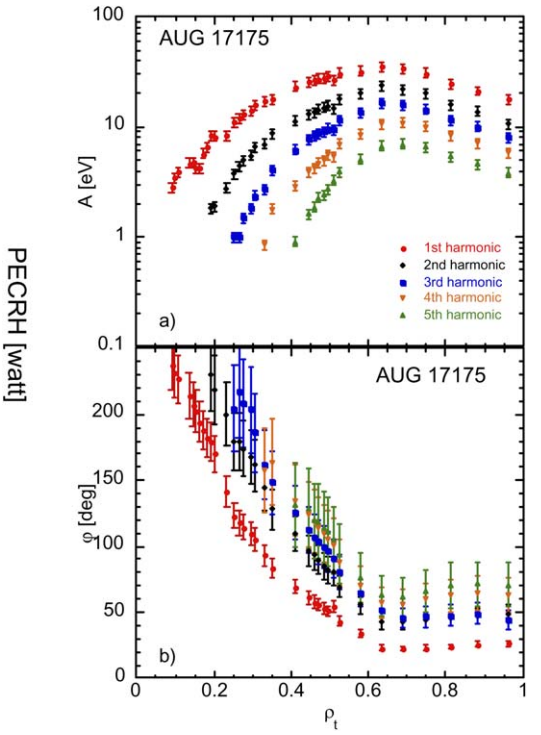

Fig. 5. Radial profiles of amplitude and phase of the T_e wave at various harmonics of the modulation frequency for the discharge of Fig. 4 ($t = 3.26$–3.94 s).

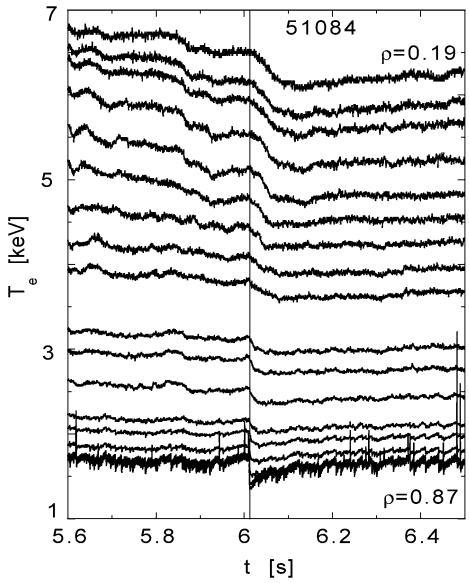

Fig. 6. Experimental time traces of electron temperature for a pellet cold pulse ($t = 6$ s) in a JET discharge with low core magnetic shear (shot 51 084). From [28].

^{3}He minority (with concentrations 3–8%) is to be preferred to H minority because of narrower power deposition and shorter slowing down, but it turns out to be a better tool for ion than for electron modulation. Instead, when ^{3}He concentration is ∼15–20%, Mode Conversion to short wavelength waves at the ion–ion hybrid layer takes place [26, 27], which provides for most power being directly absorbed by electrons with rather narrow profile. The quality of heat wave data is then not much inferior to ECH modulation, however a precise knowledge of power deposition is difficult to obtain from theoretical predictions, and so needs to be worked out experimentally from the higher frequency modulation components. This scheme is limited to high toroidal field values at the ICRH frequencies available in experiments. Control of power localization is not as straightforward as with ECH, as not only the toroidal field value but also the ^{3}He concentration determines the location of the ion–ion hybrid layer. Real Time Control of the ^{3}He concentration is therefore required in such experiments.

Finally, perturbations localized at the plasma edge and propagating to the centre have been obtained by cooling the plasma edge either by impurity injection via laser ablation of a target or by injection of D pellets with mass and speed low enough to get ablation at the plasma periphery [28–30]. The first technique is preferred for heat studies as it does not perturb the density significantly, whilst the second is used to study the simultaneous propagation of heat and particle waves, and perturbs also the ions. Fig. 6 shows T_e time traces for a D shallow pellet injection in a JET discharge with low core magnetic shear. Single or repetitive pulses can be used; we note that even with single pulses a Fourier spectrum can be extracted, given the shape of the T_e time waveform, containing a continuous range of frequencies, as discussed in [31].

3. Perturbative heat transport results in L- and H-mode plasmas

3.1. Overview of recent results in L-mode plasmas with dominant electron heating

As mentioned above, numerous investigations of electron heat pulse propagation have been carried out since the beginning of the 1980s, using heating power modulation, sawtooth pulses or cold pulses. However, until recently, the dependencies upon controlled parameters (heating power, current) or plasma parameters (density, temperature, safety factor) did not seem to be consistent between devices and appeared often disconnected from the power balance analysis. The guide-line indicated by theory that χ_e increases with R/L_{T_e} above a threshold in R/L_{T_e} and has a gyro-Bohm behaviour ($\propto T_e^{3/2}$) has brought some clarity into the picture, supported by recent experiments with flexible ECH systems. In the framework of the existence of a threshold, the possibility to deposit ECH off-axis is essential

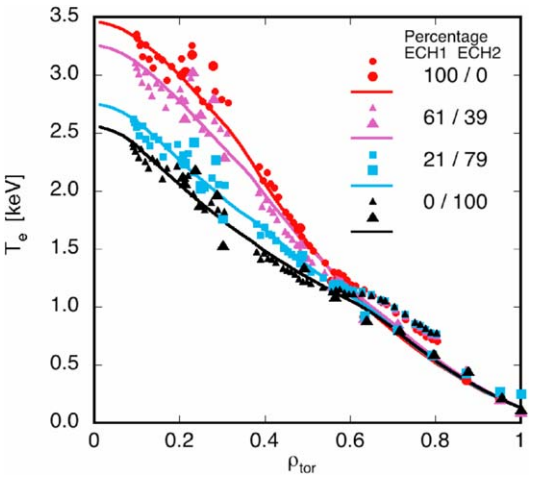

Fig. 7. T_e profile in the variation of R/L_{T_e}: data from ASDEX Upgrade and simulation with the model (after [32]).

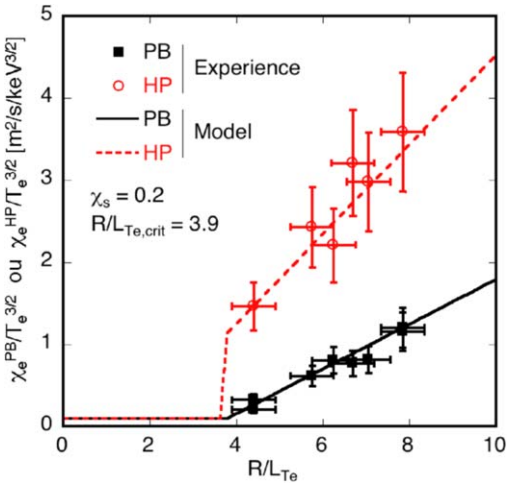

Fig. 8. Normalized values of χ_e^{PB} and χ_e^{HP} versus R/L_{T_e} at mid-radius for the discharges in Fig. 7. The lines are given by the model and deduced as explained in the text (after [32]).

because it divides the plasma into two parts. In the outer part with respect to the ECH power deposition, the heat flux is high and the temperature profile is well above the threshold. In the inner part with respect to ECH, the heat flux, provided by the residual Ohmic flux alone, from which the losses must be subtracted, is in general very low. In this case, the temperature profile is close to the threshold, and sometimes even below. If power modulation is also applied, a simultaneous analysis of steady-sate and modulation data can be carried out which yields the maximum information and also ensures the most stringent conditions for model testing. The critical gradient model described above has proved to reproduce correctly both steady-state and modulation data [19,32]. In the ideal case, applying the model to known χ_e^{PB} and χ_e^{HP} allows the determination of χ_s and $R/L_{T_{e,\mathrm{crit}}}$, if χ_0 is negligible. However, due to the experimental uncertainties and depending on the values of χ_s and $R/L_{T_{e,\mathrm{crit}}}$ the determination of these coefficients from a single shot can be very imprecise. Therefore, scanning R/L_{T_e} in a shot series, keeping T_e as constant as possible, is better suited for these studies. Such experiments have been carried out in ASDEX Upgrade using two ECH powers, P_{ECH1} and P_{ECH2}, deposited at 2 different radii, while $P_{\mathrm{ECH1}}/P_{\mathrm{ECH2}}$ was varied keeping $P_{\mathrm{ECH1}} + P_{\mathrm{ECH2}}$ constant. The value of R/L_{T_e} could be modified by a factor of 2 whereas T_e changed by only $\pm 15\%$. The T_e profiles obtained in this study are shown in Fig. 7. In the frame of the model, the analysis allows the determination of χ_s and the threshold at each radius. The results obtained at mid-radius are shown in Fig. 8.

The fit through the power balance data (black points and line) yields $\chi_s = 0.2$ and $R/L_{T_{e,\mathrm{crit}}} \approx 3.9$. Transport below the threshold is indeed low. These values reported in the expression given by the model for χ_e^{HP} agree well with the modulation data (red points and dashed line in Fig. 8). Full numerical transport simulations using the model and these values over the whole radius yield good agreement for the T_e profiles (lines in Fig. 7). The profiles of the modulation data are also well reproduced [32]. This strongly suggests that the hypothesis of the existence of a threshold is correct. Moreover, the value of 0.2 for χ_s is rather low: the electron temperature profiles are not highly stiff. In fact, as indicated by Fig. 8, the T_e profiles can exceed the threshold by a factor of 2 or 3. Gyro-kinetic stability analysis indicated that the TEM are the dominant modes [21]. Similar experiments repeated in DIII-D [33] and TCV [34] yielded comparable results.

The lowest value reached for R/L_{T_e} in these experiments remained just above the threshold due to the sufficient residual Ohmic heat flux and the low transport: the existence of a threshold could not be unambiguously demonstrated. Instead, its existence was demonstrated in similar experiments repeated at lower current in which R/L_{T_e} could be varied around $R/L_{T_{e,\mathrm{crit}}}$ [35]. Indeed, as shown in Figs. 9 and 10, both heat flux q_e and χ_e^{HP} exhibit the properties expected for the existence of a strong non-linearity of transport at a given value of R/L_{T_e}, which is characteristic of a threshold.

The heat flux dependence on R/L_{T_e} is strongly non-linear at $R/L_{T_e} \approx 3$ (Fig. 9), whereas χ_e^{HP} exhibits a jump-like behaviour there (Fig. 10). This behaviour is in accordance with a critical gradient length concept and is well

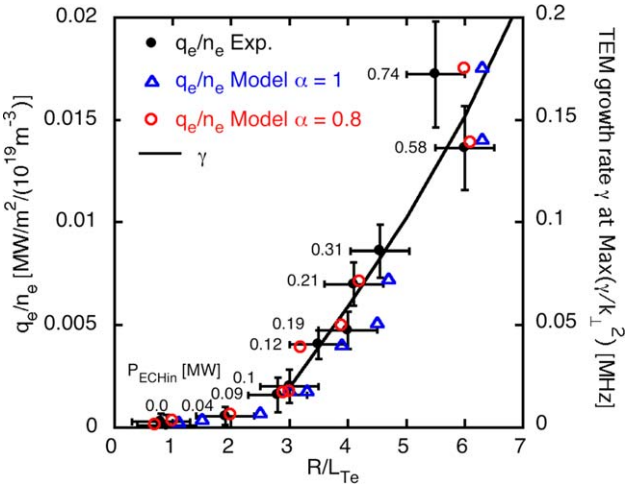

Fig. 9. Heat flux versus R/L_{T_e} in experiments showing the threshold in ASDEX Upgrade. The symbols are indicated in the legend. The line is from the gyro-kinetic calculations (after [35]).

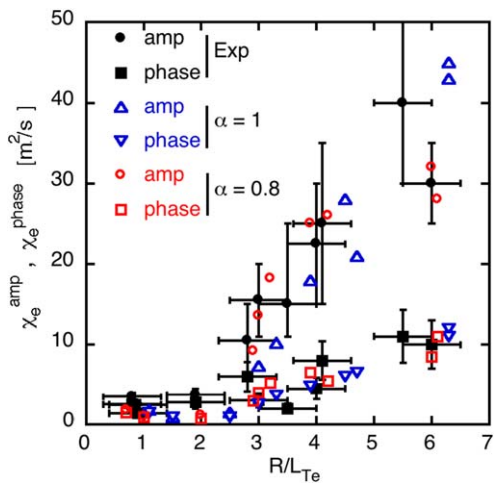

Fig. 10. χ_e^{Amp} and χ_e^{phi} deduced from amplitude and phase of the Fourier transformation for the experiments of Fig. 9. Symbols according to the legend (after [35]).

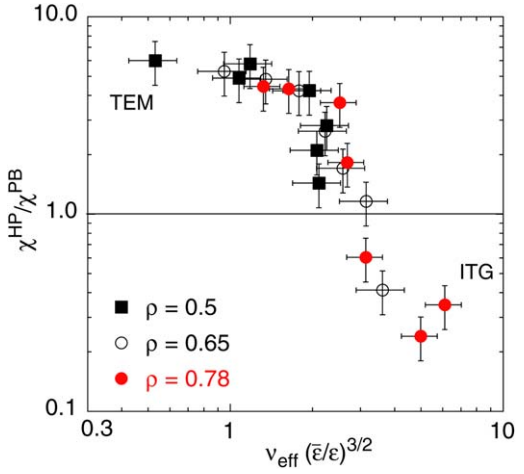

Fig. 11. Ratio $\chi_e^{\mathrm{HP}}/\chi_e^{\mathrm{PB}}$ versus normalized effective collisionality in ASDEX Upgrade, showing a behaviour consistent with the transition from TEM to ITG dominated electron heat transport (after [35]).

reproduced by the CGM empirical model, as indicated in the figures by the open symbols. In addition, the value of the threshold and the shape of the increase above it agree with gyro-kinetic stability calculation of TEM modes, as illustrated by the growth rate of the relevant mode (Fig. 9). In summary, under conditions of dominant electron heating with $T_e > T_i$, at rather low collisionality, the experimental observations are consistent with the hypothesis that electron heat transport is dominated by TEM driven turbulence.

The specific stabilization of the TEM modes at high collisionality could also be demonstrated experimentally [35]. The propagation of electron heat pulses excited by ECH has been studied versus collisionality, which was varied by the density. The analysis reveals a strong decrease of the ratio $\chi_e^{\mathrm{HP}}/\chi_e^{\mathrm{PB}}$ at $\nu_{\mathrm{eff}} \approx 2$, above which the value of $\chi_e^{\mathrm{HP}}/\chi_e^{\mathrm{PB}}$ drops below unity reaching values as low as 0.3, as shown in Fig. 11.

These results are interpreted as follows: at high collisionality the TEM modes are stabilised and the electron heat flux, which is nonzero, is driven by the ITG turbulence. The gyro-kinetic stability calculations indicate in this case that χ_e^{HP} is lower than χ_e^{PB} because the ITG- driven electron heat flux depends very weakly upon R/L_{T_e}. This does not occur for the TEM-driven heat flux for which the R/L_{T_e} dependence is always strong, yielding $\chi_e^{\mathrm{HP}}/\chi_e^{\mathrm{PB}} > 1$. As

suggested in [36], this behaviour might explain the transition between the linear and saturated Ohmic regimes. These results confirm the predicted properties for the TEM modes and indicate their crucial role in electron heat transport.

The existence of convective terms in the electron heat flux is predicted by electrostatic turbulence theories [37–39]. The possible existence of an inwardly directed convective flux (heat pinch) has been advocated for experiments made in DIII-D [40] and FTU [41] to explain the peaked T_e profiles despite strong off-axis ECH. As mentioned in Section 2.2, power modulation at low frequency permits the diagnosis of such a convective effect by the distortion of the amplitude profile. Modulation experiments carried out in RTP [42] and ASDEX Upgrade [43] show indeed that the amplitude and phase profiles yielded by the Fourier transformation of T_e for different frequencies exhibit characteristics which can be attributed to convection. However, modelling of the ASDEX Upgrade results using the CGM model shows that such distortions can also be reproduced by the model in a situation where the plasma oscillates around the threshold during modulation [43]. This effect is possibly increased by the fact that close to the threshold the temperature dependence of the model is equivalent to an inward convective term in the modulation data, as pointed out in [19]. It seems however that a small real inward convection velocity $U \sim 1$–3 m/s is also required to model the data, as discussed in detail in [43].

3.2. L- and H-modes, inter-machine comparison

The above results were obtained in L-modes with dominant electron heating. However, a large range of L- and H-plasmas are heated with NBI which provides electron and ion heating in variable proportions. In such cases, the ITG turbulence, which drives ion transport in addition to the neoclassical effects, also contributes to electron heat transport. Moreover, the ETG modes may become unstable, complicating the situation. Power modulation with electron heating has been carried out in plasmas with NBI as the main heating source, in DIII-D [44], JET [27,45] and ASDEX Upgrade [46]. In DIII-D, ECH power modulation has been applied to NBI heated L-modes. The resulting perturbation of both ion and electron temperatures could be measured, showing that T_i was out of phase compared to T_e. This is in agreement with the destabilization of the ITG modes by increasing T_e/T_i. In JET, a comparison between L- and H-mode discharges has been performed. The H-mode requires more heating power, leading to higher electron and ion temperatures and heat fluxes. The perturbative analysis suggests that χ_s in H-mode is somewhat lower than in L-mode, the difference being at most 50% [27]. This may reflect a shift of the contribution to electron heat transport from TEM to ITG modes.

In ASDEX Upgrade, electron perturbative analyses have been carried out in low collisionality H-modes with $T_i > T_e$ [46]. The analyses suggest the possible existence of a threshold and indicate that χ_s is comparable to that measured in L-mode plasmas with $T_e > T_i$ described in the previous section. In H-modes, the temperatures are significantly higher than in L-modes and the strong influence of $T_e^{3/2}$ could be clearly shown.

Based on the empirical model, an inter-machine comparison including ASDEX Upgrade, FTU, JET and Tore Supra has been carried out [20]. The values of χ_s and $R/L_{T_{e,\mathrm{crit}}}$ have been gathered. The recent results are summarized in Figs. 12 and 13, showing χ_s versus $R/L_{T_{e,\mathrm{crit}}}$ for different tokamaks and plasma types. The excursion in $R/L_{T_{e,\mathrm{crit}}}$ is large but in the expected range. The discharges with dominant electron heating yield values for χ_s in the range 0.1 to 0.5 and agree with the hypothesis that the TEM modes dominate. Those with NBI heating (electron + ion heating) cover a much larger range in χ_s, which might reflect the contributions of all three modes (ITG, TEM, ETG) depending in detail on the conditions. Fig.12 shows that the values for H-modes are within those of the L-modes. In addition, the H-mode value of χ_s are above those of the L-modes with dominant electron heating but below those of L-modes with NBI heating. This is consistent with the observation that electron transport stiffness in H-mode might be somewhat lower than in L-mode (JET), but also that χ_s might increase with ion heating due to the contribution of ITG and/or ETG modes.

3.3. Consistency between different types of perturbations

As mentioned above, the results yielded by the propagation of pulses generated by MHD events are not suitable for electron heat transport studies. Comparisons between the results deduced from cold pulses and ECH modulation have been carried out in ASDEX Upgrade [47,48] and JET [49]. In ASDEX Upgrade, the propagation of ECH induced pulses and cold pulses are not identical but exhibit similarities. In particular, the amplitude of the cold pulses launched from the plasma edge first increases over about one third of the plasma radius before decreasing, as expected from

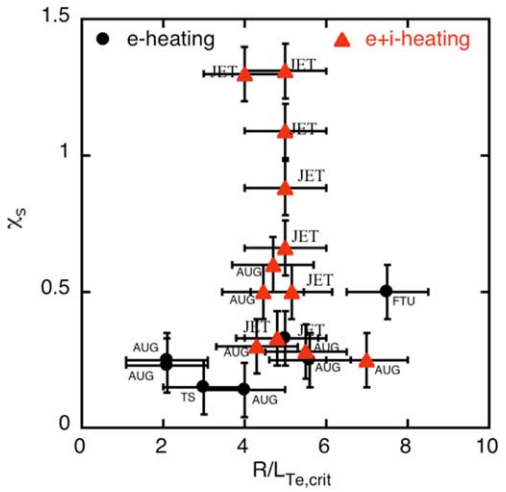

Fig. 12. Values of χ_s versus $R/L_{T_{e,\mathrm{crit}}}$ for pure electron heating and with NBI (e + i heating) in various machines.

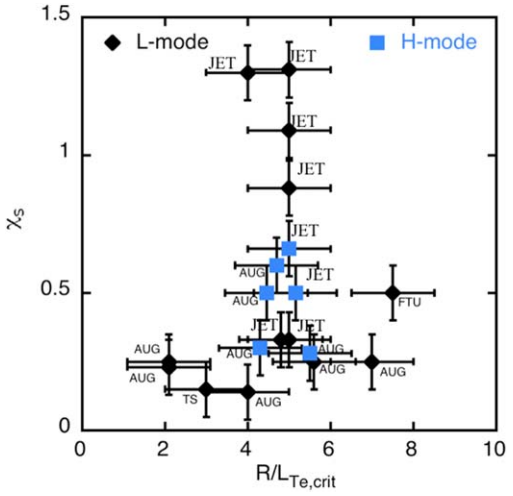

Fig. 13. Values of χ_s versus $R/L_{T_{e,\mathrm{crit}}}$ for L- and H-modes in various machines.

diffusion. This puzzling effect is not caused by convection [47]. The phase, however, behaves similarly for ECH heat pulses and cold pulses, yielding comparable values of χ_e^{φ} , i.e., similar speed of propagation. In addition, the presence of continuous ECH power at mid-radius, which determines 2 regions with quite different transport levels as discussed above, is reflected in the same way by ECH heat pulses and cold pulses. The assumption of a critical gradient model also explains the propagation of the cold pulses [48]. In JET, the behaviour of cold pulses is quite different from the picture observed in ASDEX Upgrade and is somehow at variance with respect to RF modulation heat waves. The cold pulses propagate very fast from edge to centre even when the core plasma features a large region below threshold, in which heat waves from RF modulation are observed to slow down [49]. The cold pulse in JET is only seen to slow down when a region of negative magnetic shear (reversed q profile) is present in the plasma core [28]. No physics reason has been identified so far for the fast propagation, but it should be underlined that a cold pulse produces locally a strong increase of the absolute value of R/L_{Te} and therefore a (strong) local increase of transport which might lead to the observed effect. In addition, cold pulses also create a drop of T_e/T_i which can affect ion transport though the ITG mode stability and influence the cold pulse propagation by the coupling between ion and electron channels [50].

In summary, it is believed that ECH modulation yields the most reliable results on electron heat transport and enables the assessment of the basic ideas regarding electron heat transport driven by turbulent mechanisms. However, the experiments with cold pulses indicate that the commonly used models are probably not describing the transport completely.

4. Perturbative heat transport results in plasmas with Internal Transport Barriers

Perturbative studies of plasmas characterized by the presence of Internal Transport Barriers (i.e., regions with low levels of turbulence and heat diffusivity and therefore high temperature gradients) have started only recently, with experiments carried out in JET [28,51] and JT-60U [52]. In both machines cold pulses were used, and in JET the first results of T_e modulation experiments have also been obtained. One difficulty is that perturbations coming from the edge easily destroy the ITB, so ITBs need to be well developed to be probed by cold pulses, especially by shallow pellets. Power modulation seems less critical, however one problem is the high level of MHD activity typical of ITB plasmas, which complicates the extraction of the transport relevant information from the modulated T_e time traces.

The change in propagation of the heat/cold waves when crossing the ITB is clearly visible in the data. One example is provided in Fig. 14, which illustrates a JET discharge in which off-axis T_e modulation was provided by mode conversion of ICH power, with an additional core modulation due to fast wave deposition. Two heat waves are then propagating towards the ITB from either side of it. Fig. 14(b) shows data when the ITB is present whilst Fig. 14(c) shows the same after the ITB is lost. In the latter case the propagation is smooth, whilst the ITB introduces sharp discontinuities in the slopes of A and φ profiles. This shows that indeed the ITB is spatially a well localized layer

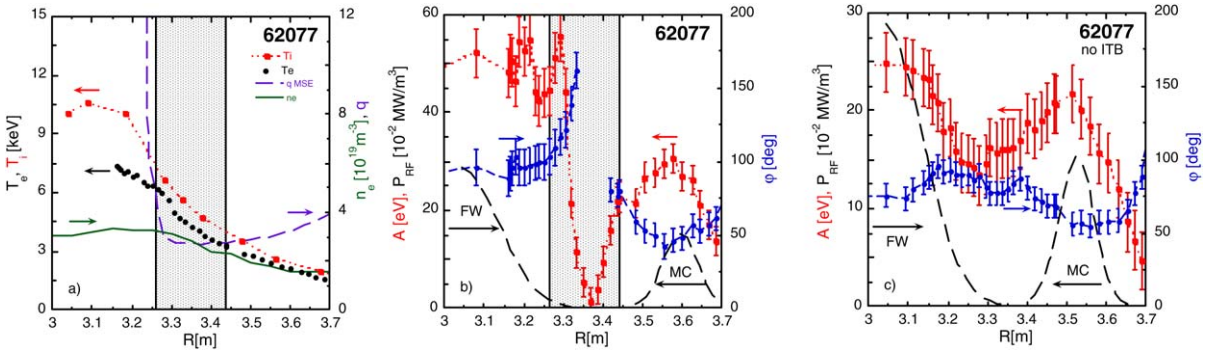

Fig. 14. (a) Experimental profiles at $t = 5.5$ s of T_e, T_i, n_e and q for JET shot 62 077 (3.25 T/2.6 MA, ^{3}He $\sim 20\%$, ICRH $f = 37$ MHz). The ITB region is highlighted. (b) Profiles of Fourier component of A (red squares) and φ (blue circles) at the modulation frequency (20 Hz) during the time interval 5.5–5.7 s. Estimated RF power deposition profiles are also plotted (dashed black line). (c) same as (b) for the time interval $t = 8$–9 s, when the ITB has been lost. From [51].

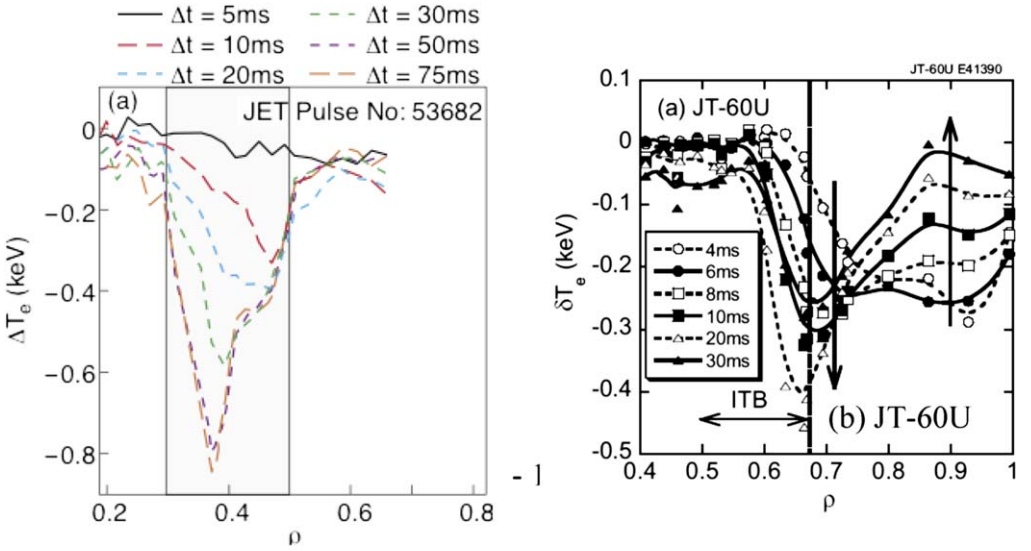

Fig. 15. Time evolution of experimental T_e variation (ΔT_e) profile following a cold pulse in ITB plasma. (a) In JET (from [28]), (b) in JT-60U (from [52]). Timing is relative to the time of cold pulse application.

(see also the discussion in [53]). The heat wave amplitude is damped strongly by the ITB layer, which indicates a low value of the perturbed heat diffusivity, consistent with a complete loss of stiffness due to the plasma having become fully sub-critical with respect to an increased threshold value. This is in contrast with a picture of the ITB as a layer with stiff transport close to a threshold higher than in conventional regimes, which would provide high values of the perturbed heat diffusivity in the ITB layer and consequently waves propagating very fast across it rather than damped by it. A model based on the same critical gradient concept as the one discussed in Section 2.3 has been found successful in reproducing the data if the ITB is modelled as a layer fully below threshold.

Cold pulses travelling towards the ITB show the peculiar feature, both in JET [28] and JT-60U [52], that the amplitude increases near the ITB outer boundary, and is then damped strongly when travelling further into the ITB layer. This is shown in Fig. 15. The interpretation proposed for this result is, however, very different in the two machines. In JET, the result is interpreted within the framework of the critical gradient model and is consistent with the modulation findings that the ITB is a layer below the critical threshold for turbulence onset: then the cold pulse driving a transient increase in gradient would induce a back-transition to a turbulent regime in the outer part of ITB, with consequent χ increase and cold pulse growth, whilst in the well stabilized inner ITB part the increase in gradient would not be enough to de-stabilize turbulence, so the low χ region would simply act to damp the cold pulse. In

contrast, in JT-60U the cold pulse growth is ascribed empirically to an inverse dependence of χ on T, inducing a χ growth when T is reduced by the cold pulse, without however proposing a physical mechanism to account for such peculiar dependence, which is at odds with the gyro-Bohm scaling of χ with T that characterizes non-ITB plasmas.

The interaction of cold pulses with ITBs actually brings precious experimental evidence on the type of transition mechanism underlying ITB formation. At present, there is an ongoing debate (see chapter on ITBs in this issue [53]) as to whether the ITB is formed via a bifurcation process (i.e., according to a 1st order transition scheme) or rather via a threshold mechanism involving a continuous dependence of the heat flux on T gradient (i.e., a 2nd order transition scheme as with a critical gradient model). It is shown in [51] that the cold pulse growth at ITB boundary favours the second hypothesis. This leads to a somewhat different picture for ITB formation with respect to the widely accepted picture for edge barrier formation in the L–H transition. For the latter, a 1st order transition is envisaged, induced by the stabilizing effect of $E \times B$ flow shear. For ITB formation, instead, stability analysis as in [54] has shown that under the assumption of neoclassical poloidal velocity, $E \times B$ flow shear is not the main player for ITB triggering. Other factors, like the presence of negative magnetic shear or of a low order rational magnetic surface at zero shear, could be responsible of ITB formation via a 2nd order process. Recently, however, a significant anomalous poloidal velocity has been measured in ITB plasmas [55]. It remains to be assessed whether the measured poloidal velocity could re-establish a dominant role of the $E \times B$ flow shear in ITB formation, and whether this could determine a 2nd order type transition scheme, consistent with the cold pulse behaviour. Non-linear 3D fluid turbulence simulations with the TRB [56] and CUTIE [57] codes have qualitatively reproduced the effect of cold pulse growth at ITB boundary and subsequent damping observed in experiment [45,53].

5. Suggestions for future work

5.1. Is transport local or non-local?

Transport driven by micro-turbulence (TEM, ITG, ETG) is in general determined by the local plasma parameters. However, the existence of radially elongated convection cells as observed in non-linear calculations of ETG turbulence, could modify the local character. Perturbative transport is the only way to address the question of the locality. Cold pulse experiments suggest, in some cases, a very fast reaction in the plasma centre to the edge cooling, raising the question as to whether transport is determined purely locally or can also be influenced at distance, through non-local phenomena (see review [58] and references therein). Whereas cold pulses induced by impurities or pellets involved complex physics mechanisms, including atomic physics at the plasma edge, ECH turn-on/turn-off experiments in the W7-AS stellarator, which also suggested a very fast transport response [59], are less complex. Although micro-turbulence driven transport seems to explain a large part of the observations, understanding the fast propagation occurring in some cases would improve the assessment of our description of transport. This probably requires non-linear time-dependent turbulence calculations for comparison with perturbative experiments which should be increasingly more accessible in the coming years. Also, alternative simplified theoretical approaches have been suggested, either based on a generalization of the transport formalism involving the use of non-Gaussian Lévy distributions [60], or based on the idea of turbulence spreading [61], in which such fast plasma responses are naturally predicted. These ideas still need to be tested thoroughly against experimental observations.

5.2. Further electron heat transport studies

If on one hand the physics underlying electron heat transport in electron heated plasmas (where TEM is the dominant instability) seems well clarified, much work remains to be done to investigate the respective roles of TEM, ITG and ETG modes in plasmas with substantial ion heating and with/without rotation, where all instabilities come into play. These are clearly the conditions relevant for ITER operation. As mentioned in Section 3.2, some observations and hints for interpretation exist but a clear understanding is not yet in place. The task is complicated and it is not yet clear how to proceed experimentally. Collecting experimental measurements of stiffness parameters in various plasma conditions is not sufficient to identify the key issues. Possibly one should try to simplify the situation for example using high collisionality to get rid of TEM. The experiments should also be strongly supported by turbulence measurements and turbulence calculations by non-linear gyrokinetics codes.

5.3. Validation of 1st principle theoretical models

Although the use of empirical models like that of Eq. (10) permits good physical insights into the plasma transport mechanisms, it is clear that only the validation of 1st principle transport models can create the physics basis for extrapolation of transport predictions to reactor conditions. An exhaustive review of this work is presented within this issue in the chapter [18]. Perturbative experiments are the most powerful test to discriminate amongst transport models, which may yield similar predictions for steady-state but very different dynamical behaviour. Much work remains to be done in this direction. 1D quasi-linear fluid models like Weiland [37] or gyro-fluid GLF-23 [62] are easy to apply to time-dependent simulations and have been found reasonably capable of reproducing electron temperature modulation results in ASDEX Upgrade [63] and JET [64] but not in all cases and definitely not for cold pulses [28]. On the other hand, non-linear 3D fluid turbulence codes are impossible to apply to simulation of the long time intervals required by modulation experiments in large machines, and very few attempts exist to apply them to modulation in small machines [38] or fast cold pulses [3,45], still implying several weeks of computing time for each case run. It is clear however that this is the way to go to gain physics insight into perturbative transport results and the continuous improvement of computing resources will make this approach more accessible. The situation in this respect is worse for non-linear gyro-kinetic codes, which are even more demanding in computing time.

5.4. Possible extensions of experimental techniques

The usefulness of perturbative experiments has been mainly demonstrated in transport investigations of impurities and electron heat. Perturbative experiments to investigate transport of electrons as particles are fewer, due essentially to the lack of a local and fast measurement of electron density. It is envisaged that improvement of reflectomer techniques would allow new experiments to extract interesting information on the thermo-diffusion and curvature terms of particle convection [65]. An interesting preliminary result in this direction has been obtained with reflectometer measurements of the local density response to electron temperature modulation on Tore Supra [66]. Perturbative studies of ion heat and momentum transport have been started, made possible by the increased time resolution available for Charge Exchange diagnostics, measuring ion temperature and plasma rotation profiles. The main challenge here remains the lack of a localized source. For the ion heat, it is expected that use of ICRH ^{3}He minority will allow fruitful experiments for which the experience gained in electron heat transport studies can be directly transposed. NBI modulation for perturbative momentum studies is a totally new issue to explore, as well as current diffusion via modulation of current drive, which requires improvement of local current density measurements.

6. Conclusions

Perturbative techniques are a powerful tool to explore the physics of transport, and have been extensively used to study electron heat and impurity transport. Diagnostic improvements will soon allow their use also for ion heat, main particle and momentum transport.

In the field of electron heat transport, power modulation studies have allowed a thorough assessment of the concept that a threshold exists in the inverse temperature gradient length, above which transport driven by electrostatic turbulence modes sets up, thereby preventing the temperature profile to depart significantly from threshold—the so called temperature profile stiffness. The heat waves clearly show a change in propagation properties when crossing the threshold, with a discontinuous jump of the incremental (perturbative) heat diffusivity that becomes significantly larger than the power balance one. The transition from below to above threshold can be observed at a given radius for a series of discharges with varying electron power deposition profile, or within the same discharge across the radial profile following the increase in heat flux from centre to edge.

With the help of simple semi-empirical models, power modulation provides a unique tool to determine threshold and stiffness levels and investigate their parametric dependences or compare amongst different machines. Threshold values have been found in the right ball-park for ITG/TEM modes, and stiffness levels have been observed to vary significantly with plasma parameters: for example pure electron heated plasmas are observed to have a lower degree of stiffness than plasmas with mixed ion and electron heating. The transition from TEM dominated to ITG dominated transport with increasing collisionality has also been diagnosed on the basis of the change of propagation properties of the heat waves.

The dynamic response of the temperature profile to power modulation provides a much more stringent experimental constraint for the validation of theoretical transport models than steady-state data alone. This will be even more important when also good ion heat transient data will become available. The possibility of validating physics based models is of crucial importance in view of extrapolation to ITER. In particular, ITER performance in standard ELMy H-mode depends on the achievement of high core temperatures. This is highly dependent on the stiffness properties of the plasma (threshold and stiffness level) since the pedestal height cannot be arbitrarily increased beyond the first wall capabilities to sustain ELM generated heat loads. From the elements we have so far, it seems that a significant level of stiffness is to be expected in ITER plasmas, characterized by low collisionality and high electron and ion heating, although a proper effort of theory validation against perturbative data is very much on-going and therefore precise quantitative predictions cannot yet be made. Also features like non-locality or the existence of pinches, for which experimental evidence from perturbations exists, and which are now most commonly ignored, will have to be consistently incorporated in a theoretical transport model that aims at reliably predicting ITER transport properties.

Finally, perturbative electron heat transport studies have recently been carried out in plasmas with Internal Transport Barriers, pointing out the narrow spatial extent of the ITB layer. Strong attenuation of the heat waves by the ITB indicates that transport in the ITB layer is below the turbulent threshold for ITG/TEM. Also in this case perturbative techniques have proved a unique tool to discriminate between various hypotheses of physics mechanisms that would be indistinguishable from pure steady-state analysis. Such understanding is of vital importance for any extrapolation of regimes with ITBs to future machines.

Future work will most certainly bring more refined measurements of the plasma dynamic response, extended to all transport channels. It is important to stress here that this needs to be accompanied by a more vigorous theoretical effort to address the perturbative results and exploit their large amount of additional information in order to achieve the target of a validated comprehensive tool for transport predictions in future machines.

References

[1] K.W. Gentle, B. Richards, F. Waelbroeck, Plasma Phys. Control. Fusion 29 (1987) 1077.
[2] L. Garzotti, et al., Nucl. Fusion 43 (2003) 1829.
[3] L. Garzotti, et al., Nucl. Fusion 46 (2006) 73.
[4] R. Dux, Nucl. Fusion 39 (1999) 1509.
[5] R. Dux, et al., Plasma Phys. Control. Fusion 45 (2003) 1815.
[6] R. Dux, et al., Nucl. Fusion 44 (2004) 260.
[7] M.E. Puiatti, et al., Phys. Plasmas, in press.
[8] C. Giroud, et al., in: Proceedings of 31st EPS Conference, London, 2004, in: Europhysics Conference Abstracts, vol. 28G, European Physical Society, 2004, P1.144.
[9] K.D. Zastrow, et al., Plasma Phys. Control. Fusion 46 (2004) B255.
[10] X. Garbet, Introduction to turbulent transport in fusion plasmas, C. R. Physique 7 (2006), this issue.
[11] N.J. Lopes Cardozo, et al., Plasma Phys. Control. Fusion 32 (1990) 983.
[12] N.J. Lopes Cardozo, Plasma Phys. Control. Fusion 37 (1995) 799.
[13] U. Stroth, Plasma Phys. Control. Fusion 40 (1998) 9.
[14] F. Ryter, et al., Plasma Phys. Control. Fusion 43 (2001) A323.
[15] K.W. Gentle, Phys. Fluids 31 (1988) 1105.
[16] B. Tubbing, et al., Nucl. Fusion 27 (1987) 1843.
[17] A. Jacchia, et al., Phys. Fluids B 3 (1991) 3033.
[18] A.G. Peeters, C. Angioni, G. Tardini, Transport modelling, C. R. Physique 7 (2006), this issue.
[19] F. Imbeaux, et al., Plasma Phys. Control. Fusion 43 (2001) 1503.
[20] X. Garbet, et al., Plasma Phys. Control. Fusion 46 (2004) 1351.
[21] A.G. Peeters, Phys. Plasmas 12 (2005) 022505.
[22] J.D. Callen, G.L. Jahns, Phys. Rev. Lett. 38 (1977) 491.
[23] Y. Sarazin, et al., Plasma Phys. Control. Fusion 44 (2002) 2445.
[24] E.D. Fredrickson, et al., Phys. Rev. Lett. 65 (1990) 2869.
[25] F. Leuteter, et al., Nucl. Fusion 43 (2003) 1329.
[26] M. Mantsinen, et al., Nucl. Fusion 44 (2004) 33.
[27] P. Mantica, et al., in: Proceedings of 30th EPS Conference, St. Petersburg, 2003, in: Europhysics Conference Abstracts, vol. 27A, European Physical Society, 2003, O-3.1A.
[28] P. Mantica, et al., Plasma Phys. Control. Fusion 44 (2002) 2185.
[29] F. Ryter, et al., Nucl. Fusion 40 (2000) 1917.
[30] M.W. Kissick, et al., Nucl. Fusion 34 (1994) 349.

[31] P. Mantica, et al., Nucl. Fusion 32 (1992) 2203.
[32] F. Ryter, et al., Nucl. Fusion 43 (2003) 1396.
[33] J.C. DeBoo, et al., Nucl. Fusion 45 (2005) 494.
[34] Y. Camenen, Plasma Phys. Control. Fusion 47 (2005) 1971.
[35] F. Ryter, et al., Phys. Rev. Lett. 95 (2005) 085001-1.
[36] C. Angioni, et al., Phys. Plasmas 12 (2005) 040701-1.
[37] J. Weiland, Collective Modes in Inhomogeneous Plasma, Kinetic and Advanced Fluid Theory, IoP Publishing, Bristol and Philadelphia, 2000.
[38] P. Mantica, et al., Phys. Rev. Lett. 95 (2005) 185002.
[39] X. Garbet, et al., Phys. Plasmas 12 (2005) 082511.
[40] T.C. Luce, et al., Phys. Rev. Lett. 68 (1992) 52.
[41] C. Sozzi, et al., in: Proceedings of the 18th International Conference on Fusion Energy, Sorrento, 2000, International Atomic Energy Agency (IAEA), Vienna, 2000, EX/P5-13.
[42] P. Mantica, et al., Phys. Rev. Lett. 85 (2000) 4534.
[43] P. Mantica, et al., Plasma Phys. Control. Fusion 48 (2006) 385.
[44] J.C. DeBoo, et al., Nucl. Fusion 39 (1999) 1935.
[45] P. Mantica, et al., in: Proceedings of the 20th International Conference on Fusion Energy, Vilamoura, 2004, International Atomic Energy Agency (IAEA), Vienna, 2004, EX/P6-18.
[46] A. Manini, et al., Plasma Phys. Control. Fusion 46 (2004) 1723.
[47] F. Ryter, et al., Nucl. Fusion 40 (2000) 1917.
[48] A. Jacchia, Nucl. Fusion 45 (2005) 40.
[49] P. Mantica, et al., in: Proceedings of the 19th International Conference on Fusion Energy, Lyon, 2002, International Atomic Energy Agency (IAEA), Vienna, 2002, EX/P1-04.
[50] J.E. Kinsey, et al., Phys. Plasmas 5 (1998) 3974.
[51] P. Mantica, et al., Phys. Rev. Lett. 96 (2006) 095002.
[52] S. Inagaki, et al., Nucl. Fusion 46 (2006) 133.
[53] T. Tala, X. Garbet, JET EFDA contributors, Physics of Internal Transport Barriers, C. R. Physique 7 (2006), this issue.
[54] X. Garbet, et al., Nucl. Fusion 43 (2003) 975.
[55] K. Crombè, et al., Phys. Rev. Lett. (2005).
[56] X. Garbet, et al., Phys. Plasmas 8 (2001) 2793.
[57] A. Thyagaraja, et al., Eur. J. Mech. B/Fluids 23 (2004) 475.
[58] J. Callen, et al., Plasma Phys. Control. Fusion 39 (1997) B173.
[59] U. Stroth, Plasma Phys. Control. Fusion 38 (1996) 611;
U. Stroth, Plasma Phys. Control. Fusion 38 (1996) 1087 (Corrigendum).
[60] B. van Milligen, et al., Plasma Phys. Control. Fusion 47 (2005) B743.
[61] V. Naulin, et al., Phys. Plasmas 12 (2005) 122306.
[62] R.E. Waltz, et al., Phys. Plasmas 4 (1997) 2482.
[63] G. Tardini, et al., Nucl. Fusion 42 (2002) L11.
[64] P. Mantica, et al., in: Proceedings of 31st EPS Conference, London, 2004, in: Europhysics Conference Abstracts, vol. 28G, European Physical Society, 2004, P1.153.
[65] X. Garbet, et al., Plasma Phys. Control. Fusion 46 (2004) B557.
[66] G.T. Hoang, et al., Nucl. Fusion 46 (2006) 306.